

Effect of global ocean temperature change on deep ocean ventilation

A. M. de Boer,^{1,2} D. M. Sigman,³ J. R. Toggweiler,⁴ and J. L. Russell^{5,6}

Received 10 November 2005; revised 21 October 2006; accepted 18 December 2006; published 9 May 2007.

[1] A growing number of paleoceanographic observations suggest that the ocean's deep ventilation is stronger in warm climates than in cold climates. Here we use a general ocean circulation model to test the hypothesis that this relation is due to the reduced sensitivity of seawater density to temperature at low mean temperature; that is, at lower temperatures the surface cooling is not as effective at densifying fresh polar waters and initiating convection. In order to isolate this factor from other climate-related feedbacks we change the model ocean temperature only where it is used to calculate the density (to which we refer below as “dynamic” temperature change). We find that a dynamically cold ocean is globally less ventilated than a dynamically warm ocean. With dynamic cooling, convection decreases markedly in regions that have strong haloclines (i.e., the Southern Ocean and the North Pacific), while overturning increases in the North Atlantic, where the positive salinity buoyancy is smallest among the polar regions. We propose that this opposite behavior of the North Atlantic to the Southern Ocean and North Pacific is the result of an energy-constrained overturning.

Citation: de Boer, A. M., D. M. Sigman, J. R. Toggweiler, and J. L. Russell (2007), Effect of global ocean temperature change on deep ocean ventilation, *Paleoceanography*, 22, PA2210, doi:10.1029/2005PA001242.

1. Introduction

[2] Deep ocean ventilation is fundamental to climate change for two reasons. First, surface waters that feed polar convection regions can come from the low latitudes and carry large amounts of heat. The overturning circulation in the North Atlantic is the most striking and well studied example; heat transported from the tropics contributes to a milder European climate [Manabe and Stouffer, 1997]. Second and equally important is the role of deep ocean ventilation in setting the concentration of atmospheric CO₂. When nutrient-rich deep water upwells to the surface, CO₂ is outgassed to the atmosphere. At the same time, surface nutrients that fuel biological productivity are refreshed. Phytoplankton growth and the associated downward rain of organic carbon recapture a portion of the upwelled dissolved inorganic carbon (DIC). However, because consumption of the upwelled nutrients is incomplete in at least some polar surface waters (the Antarctic and subarctic North Pacific in particular), the net effect of overturning (i.e., vertical exchange processes such as upwelling, convection and deep water formation) in these regions is to release some of the excess CO₂ that was sequestered in the

ocean interior by lower latitude biological productivity. Thus it has been posited that past changes in atmospheric CO₂, such as over glacial/interglacial cycles, were driven by changes in sinking and upwelling in these polar regions [Francois et al., 1997; Haug et al., 1999; Knox and McElroy, 1984; Sarmiento and Toggweiler, 1984; Siegenthaler and Wenk, 1984; Toggweiler, 1999].

[3] While consensus has not been reached, we feel that a growing number of paleoceanographic measurements suggest that the ventilation of the deep ocean through the polar ocean surface was reduced during colder times over the last 3 million years. A recent reconstruction indicates that, during the last ice age, atmospheric ¹⁴C content was much higher than it has been during the Holocene, which may have been the result of reduced deep ocean ventilation [Hughen et al., 2004]. Symmetrically, while arguments have recently been made to the contrary [Broecker et al., 2004], there are a number of indications that the deep ocean had less ¹⁴C during the last ice age. The radiocarbon age of the deep North Atlantic (NA) was dramatically higher during the last ice age than the Holocene [Keigwin, 2004], and some data indicate the same change for the deep Southern Ocean (SO) and Pacific [Adkins and Boyle, 1997; Goldstein et al., 2001; Shackleton et al., 1988; Sikes et al., 2000]. Other indications of reduced deep ocean ventilation include the accumulation of authigenic uranium in Antarctic sediments during the last glacial maximum, when productivity was reduced in the region, which suggests lower bottom water O₂ at that time [Francois et al., 1997]. As with the Antarctic uranium data, the extremely low ^δ¹³C of SO deep water in the glacial ocean suggests higher concentrations of dissolved inorganic carbon and nutrients from regeneration, consistent with reduced ventilation in this region [Charles and Fairbanks, 1992; Ninnemann and Charles, 2002].

[4] Support for a glacial decrease in deep ocean ventilation arises from studies indicating increased upper ocean

¹Cooperative Institute for Climate Science, Princeton University, Princeton, New Jersey, USA.

²Now at School of Environmental Science, University of East Anglia, Norwich, UK.

³Department of Geosciences, Princeton University, Princeton, New Jersey, USA.

⁴Geophysical Fluid Dynamics Laboratory, NOAA, Princeton, New Jersey, USA.

⁵Cooperative Institute for Climate Science, Princeton University, Princeton, New Jersey, USA.

⁶Now at Department of Geosciences, University of Arizona, Tucson, Arizona, USA.

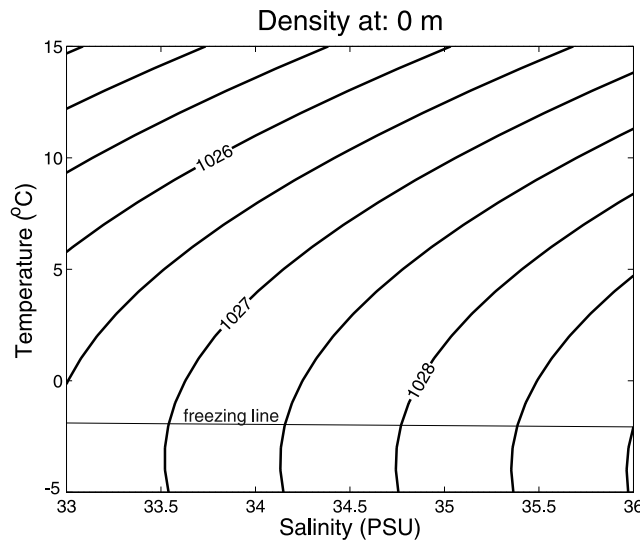


Figure 1. Seawater equation of state at the ocean surface. Contours of density are plotted every 0.5 kg m^{-3} . At cool temperatures the slopes of the density contours tend toward the vertical, indication that temperature change in this range has very little effect on density. The freezing line denotes the sensitivity of the freezing temperature to salinity.

stability in polar ocean regions (“polar stratification”). While the initial focus was on the polar NA and the evidence for reduced North Atlantic Deep Water (NADW) formation [Boyle and Keigwin, 1982], more recent work has suggested that both the Antarctic Zone of the SO and the subarctic North Pacific (SNP) became more vertically stable during the glacial maxima [Brunelle *et al.*, 2007; Francois *et al.*, 1997; Jaccard *et al.*, 2005; Robinson *et al.*, 2004]. There is similar evidence for an increase in the upper ocean stratification of both the SNP and the Antarctic at the onset of major Northern Hemisphere glaciation at 2.7 Ma [Haug *et al.*, 1999, 2005; Sigman *et al.*, 2004], as well as glacial/interglacial variations in SNP stratification immediately after that climate transition [Sigman *et al.*, 2004]. A reduction in deep ocean ventilation from the early warm Pliocene into the colder Pleistocene is also indicated by benthic foraminiferal $\delta^{13}\text{C}$ data from the North Pacific [Ravelo and Andreasen, 2000] and Southern Ocean [Hodell and Venz-Curtis, 2006].

[5] What physical mechanism could drive stratification upon global cooling? We investigate here the possibility that the answer lies in the nonlinearity of the seawater equation of state, in which the dependence of density on temperature relative to its dependence on salinity is diminished at lower temperatures (Figure 1). For instance, a water parcel at the surface that has a salinity of 35 psu would experience an increase in its density of 0.5 kg m^{-3} if it were to cool from 1°C to 0°C . The same water parcel would become denser by 1 kg m^{-3} if its temperature dropped from 4°C to 3°C . In contrast, the partial derivative of density to salinity, $\partial\rho/\partial S$, is relatively insensitive to temperature. It increases slightly (by less than 3%) when the temperature cools from 9°C to 0°C , a change that is very small but also contributes to

enhance stratification upon cooling by enhancing the fresh-water stabilization in the polar regions. The sensitivity of the equation of state (EOS) to mean temperature change can affect global ventilation in the following way.

[6] Polar regions are stratified by the low salinity of their surface waters, but sufficient winter cooling and sea ice formation can destabilize the water column and initiate deep convection. At the freezing point, the change in density with temperature, $\partial\rho/\partial T$, approaches $0 \text{ kg m}^{-3} \text{ }^\circ\text{C}^{-1}$. In this limit, the surface thermal forcing becomes impotent, and convection cannot occur if a fresh surface layer exists. In contrast, a uniform warming of the ocean would increase $\partial\rho/\partial T$ and thereby ease the destabilization of the water column in winter, promoting the formation of deep water. It should be noted that the partial derivative of density to temperature, $\partial\rho/\partial T$, is depth-dependent, as is its sensitivity to temperature. While $\partial\rho/\partial T$ increases roughly by 200% across a temperature range of 9°C at the surface, it will increase only by 40% over the same range at 4 km depth. Thus the EOS effect of a uniform temperature change may have a more direct impact on exchange between the ocean surface and the interior than on the water mass structure of the deep ocean.

[7] The effect of the mean temperature on density may also be visible in the vertical structure of the geostrophic currents. Geostrophic current shears are balanced by across-stream density gradients through the thermal wind relation. If an unchanging reference level exists (e.g., level of no motion), and if the flow above this level is moving in accordance with the temperature-induced density gradient (cold water on the right in the Southern Hemisphere), one can expect an increase in the transport above the reference level with an increase in mean temperature. The strong Antarctic Circumpolar Current (ACC) does have a strong baroclinic component of this type but does not exhibit a clear level of no motion. Nevertheless, for similar across-stream temperature and salinity gradients, one would expect a stronger vertical gradient in the current speed in warm climates, so that, if the bottom velocity remains similar, the ACC transport would be higher in warm climates.

[8] Wang *et al.* [2002] studied the response of the Atlantic overturning circulation to a cold climate. They used a climate model of intermediate complexity in which they simulated cold climates by increasing the planetary emissivity uniformly. They found that NADW formation is increased for a small climate cooling, but the trend then reverses, with the overturning collapsing at an atmospheric mean temperature of about 7°C . Their model includes various feedback mechanisms associated with a colder climate, such as increases in sea and land ice and a weaker freshwater cycle, making it difficult to distinguish the effect of the nonlinearity of the EOS.

[9] Winton [1997] used a more idealized model intended to focus on the effect of ocean cooling on NADW formation. In a two-dimensional (depth and latitude) model of the Atlantic, he finds a decreased NA overturning associated with colder climates, accompanied by an increase in SO ventilation. We compare our results with his and interpret differences in the discussion below (section 4.1). Models of the overturning during warmer climate scenarios abound.

However, as with the glacial simulations, feedback processes make it difficult to determine the effect of the mean oceanic temperature. In addition, these models are often not run for a sufficiently long time to allow the deep ocean to equilibrate. In general but not always [Stouffer and Manabe, 2003], global warming models find a reduction in NADW formation in a warmer world, a response that is explained as the result of a more vigorous hydrological cycle [Manabe and Stouffer, 1993; Rahmstorf and Ganopolski, 1999; Sarmiento et al., 1998].

[10] Here we investigate both climate warming and cooling scenarios, but, using a novel approach, we restrict ourselves to the dynamical effect of changes in the mean temperature of the ocean. To minimize interference from thermodynamic feedbacks such as the hydrological cycle, sea ice, or surface temperature gradients shifts, we systematically adjust the ocean temperature (or, more precisely, the potential temperature) only in the model routines where the density is calculated. In this way, we isolate the effect that a change of mean ocean temperature will have on the ocean circulation because of the nonlinearity of the equation of state. Further details of our experimental setup are given in section 2, together with a description of the model. The results are presented in section 3 and show the postulated ventilation changes in the SO and SNP but an unexpected response in the NA. In section 4, we interpret these findings and suggest that they can be explained by an energy-driven constraint on the global upwelling. We also compare our results with paleoceanographic observations.

2. Details of Numerical Study

2.1. Model Description

[11] The experiments are performed using an ocean general circulation model coupled to a two-dimensional energy moisture balance model (EMBM) for the atmosphere. Communication between the ocean and atmosphere is facilitated by a thermodynamic-dynamic sea ice model.

[12] The ocean model is based on the Geophysical Fluid Dynamics Laboratory's modular ocean model version 4 (MOM4 [Griffies et al., 2003]). It has a grid resolution of $4^\circ \times 4^\circ$ in the horizontal and 24 levels in the vertical. The top 120 m are composed of 8 layers of 15 m each, leaving 16 uneven layers for the remaining 4880 m. The basin geometry is idealized. It is similar to Bjornsson and Toggweiler [2001], with landmasses at both poles and two rectangular ocean basins (Figure 2). The basin representing the Indo-Pacific has double the width of the Atlantic basin. Below, we refer to the Indo-Pacific basin simply as the Pacific. The continents that separate the basins are long, thin landmasses reaching from the northern polar island to the lower latitudes of Africa and South America. An array of bottom ridges, 2500 m deep, is included to dissipate energy [Bjornsson and Toggweiler, 2001]. Their primary purposes are to slow down the ACC current and to allow Antarctic bottom water to flow northward across Drake Passage. Horizontal tracer mixing and diffusion occurs according to the schemes of Gent and McWilliams [1990] and Redi [1982] as implemented in MOM4 by Griffies [1998]. The Gent-McWilliams and Redi coefficients are both set

to $0.8 \times 10^3 \text{ m}^2 \text{ s}^{-1}$. Vertical diffusion increases from $0.1 \times 10^{-4} \text{ m}^2 \text{ s}^{-1}$ at the surface to $1.2 \times 10^{-4} \text{ m}^2 \text{ s}^{-1}$ in the deep ocean according to the profile suggested by Bryan and Lewis [1979]. The zonal component of zonally averaged ECMWF winds is applied at the surface [Trenberth et al., 1990]. In the model, there is no meridional wind stress forcing on the ocean surface. The equation of state, based on the work of McDougall et al. [2003], is fully nonlinear and computes the in situ density and its partial derivatives with respect to potential temperature and salinity.

[13] The atmospheric model is a one-layer, two-dimensional (longitude by latitude) spectral EMBM developed at GFDL. It solves two prognostic equations for temperature and the mixing ratio. At the top, it is forced by seasonally varying shortwave radiation which, at steady state, is balanced by outgoing longwave radiation. Atmospheric temperatures are a function of the surface and top radiation fluxes, lateral diffusion, and latent heat released when precipitation is formed. The mixing ratio (humidity) depends on evaporation from the ocean, precipitation and lateral diffusion. When it exceeds the temperature-dependent saturation mixing ratio, the water vapor condenses and precipitates. The EMBM has been run before by Gerdes et al. [2006] in a freshwater hosing study, but they overrode the model's freshwater flux with prescribed precipitation. This study is the first application using both the heat and freshwater fluxes derived from the EMBM and, hence we provide details of the model in Appendix A.

[14] Ocean and atmosphere are coupled by the GFDL Sea Ice Simulator [Winton, 2000], an ice model that consists of two ice layers (of variable thickness) and one snow layer. The land model is described by Milly and Shmakin [2002], but configured with globally constant soil and vegetation and no glaciers. These are set so that the land albedo varies between 0.65 and 0.8 when the surface is snow covered and is 0.15 when clear. Precipitation that falls on land runs off to the nearest ocean point.

2.2. Experiment Setup

[15] We isolate the effect that mean oceanic temperature change has on density (and in turn on the circulation) in the following way. When the model calculates the density of the seawater through the fully nonlinear equation of state, it uses as input the model temperature, salinity and pressure. At the beginning of the routine we adjust this temperature by an amount δT so that the model calculates the density of the ocean state at a temperature $(T + \delta T)$, where T is the model derived temperature and δT is -3 , -2 , 0 , 1.5 , 3 , 4.5 , 6 and 9°C in the eight respective experiments, $\delta T = 0^\circ\text{C}$ being the control run. At the end of the density routine, we subtract δT again so that the temperature is reset to the model temperature. We refer to this temperature, $T_d = T + \delta T$, at which the density is evaluated, as the dynamic temperature. In this framework, T_d determines only the dynamic properties of the model and has no direct effect on sea ice formation, evaporation or the atmospheric temperature. If we had changed the real temperature T (for instance, by adjusting the incoming radiation), it would have affected all of the above thermodynamic properties and also would have changed the

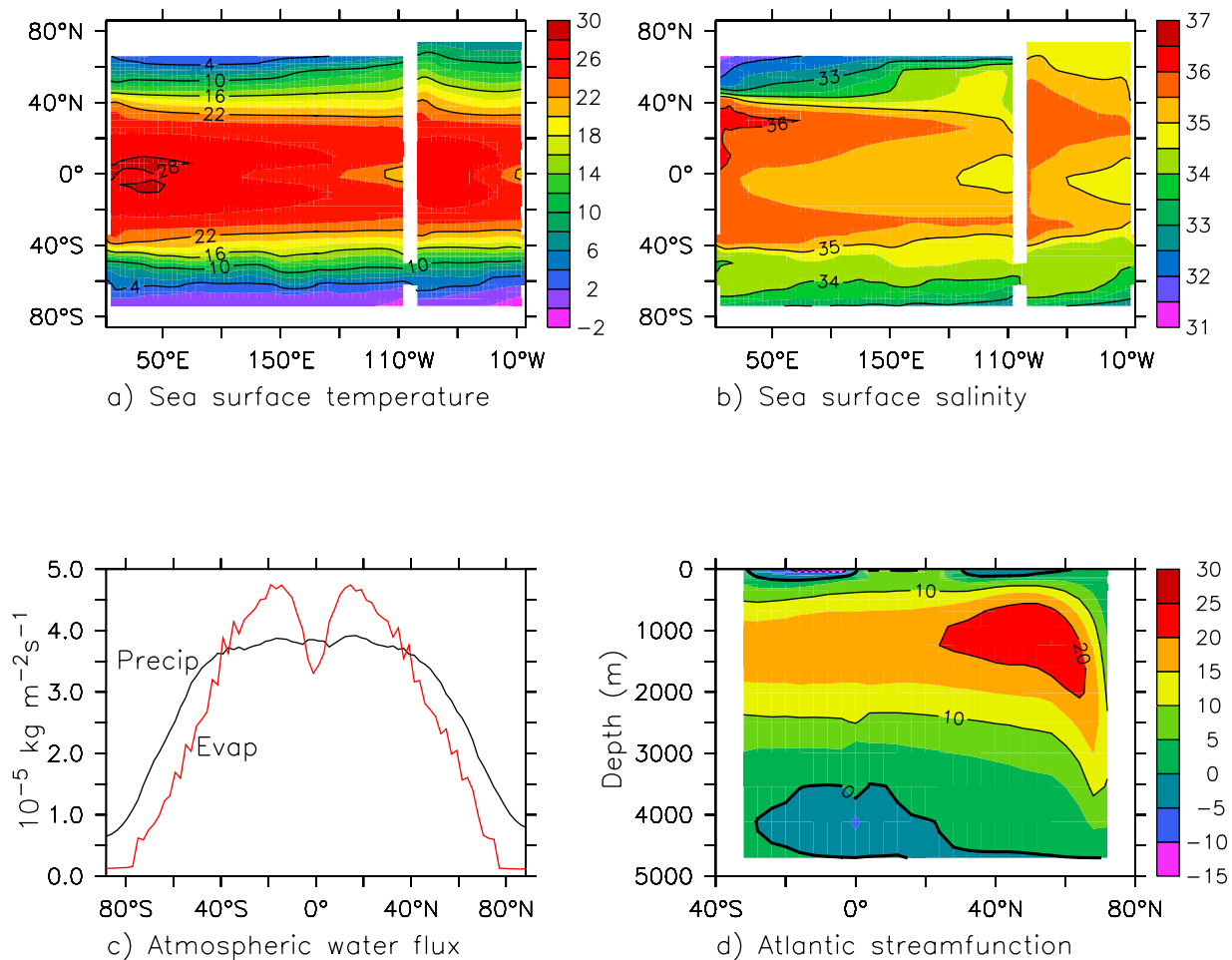


Figure 2. Diagnostics of the annually averaged model control state.

temperature gradients. In such global cooling or warming experiments, it is very difficult to distinguish the role of the equation of state from the multitude of other feedback mechanisms. Another way of thinking about the dynamic temperature adjustment is that we are tuning the equation of state so that the degree to which the density is sensitive to temperature varies in each run (higher sensitivity for higher dynamic temperature).

[16] In the model, during winter, the surface temperature in the polar regions (with the exception of the NA) reaches the freezing point of about -2°C . An additional drop of 3°C would set T_d at -5°C , that is, below the freezing point. The equation of state is not physical in this range, but the values and gradients of density continue smoothly beyond the seawater freezing point so that no major disturbances are expected. Also, it is common for the equation of state to be evaluated in this supercooled range in the multitude of ocean model experiments that do not include a sea ice model [Toggweiler and Samuels, 1995; Winton, 1997]. Nevertheless, it is exactly in these very cold regions of our model domain that one might expect deep convection to occur. To evaluate the extent to which this unrealistic temperature range influences our results, we perform an

additional experiment in which we decrease the temperature by 3°C everywhere but set the minimum T_d at -2°C . The penalty in this “fix” is that all the temperature gradients in the -2°C to 1°C (real temperature) range are not just diminished, but eliminated (i.e., all temperatures less than 1°C are set to -2°C in the density equation). As a result, nothing can prevent the negative vertical salinity gradient from setting a stable stratification. One would expect such a response if the real oceanic temperature were to decrease globally, but it simulates a feedback that is related to the temperature limit associated with freezing [Gildor *et al.*, 2002] rather than just the change of $\delta\rho/\delta T$ with T . Also, even though it is akin to a model that freezes at the correct temperature of -2°C , it does not produce sea ice and the corresponding feedbacks that are pertinent in this limit. Although neither of the two experiments at $\delta T = -3^{\circ}\text{C}$ is ideal, we will see that the model results are insensitive to the specific approach taken.

[17] Each model run is spun up from a state of horizontally homogenous temperature and salinity that was derived by averaging in each horizontal direction the fields from the National Oceanic Data Center’s World Ocean Atlas as updated by Steele *et al.* [2001]. A steady state is reached

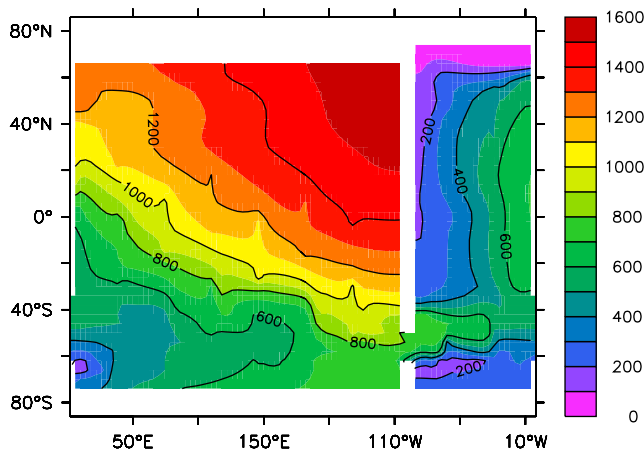


Figure 3. Ventilation age (in years) of the control run at 2500 m depth showing a core of old water in the eastern NP (annual mean distribution). Young deep water forming in the SO is more evident in the NP at greater depths, while NADW flows southward along the western boundary of the Atlantic basin.

after about 1200 years, but all the experiments were run out for 3000 years.

3. Model Results

3.1. Control Run

[18] In this paper we present the first study of MOM4 coupled to an EMBM and a sea ice model in such an idealized geometry; therefore it is appropriate to discuss briefly the behavior of the control run. Although the model is forced with seasonal solar radiation, the results described in this section are all annual averages. Given the simplicity of the model setup, the basic oceanic features are captured well. Sea surface temperatures range from -2°C at the poles to 32°C in the western equatorial Pacific (Figure 2a). Wind-driven upwelling in the eastern equatorial Pacific reduces temperatures there to 17°C . The coldest surface waters are in the SO, followed by that in the North Pacific (NP). As expected, the NA is warmed by cross equatorial heat transport because of the meridional overturning circulation there. The polar sea surface salinities exhibit a related pattern (Figure 2b) of very fresh water in the SO (33 psu) and NP (32 psu), with saltier water in the NA (35 psu). However, counter to observations, our saltiest water is found in the subtropical western NP and not in the Atlantic, presumably because of the lack of a broad Eurasian landmass to channel precipitation back into the western tropical Pacific. The average precipitation in the model, $3.40 \times 10^{-5} \text{ kg m}^{-1} \text{ s}^{-1}$, is consistent with the Ocean Modeling Intercomparison Project [Roske, 2006] data value of $3.39 \times 10^{-5} \text{ kg m}^{-1} \text{ s}^{-1}$, although our atmospheric model renders the pattern more diffuse: Water vapor is not advected by winds (but only laterally diffused), so that strong convection zones are absent (Figure 2c).

[19] The overturning in the NA fills the Atlantic basin between 1.5 and 3.5 km and its the maximum stream function of 25 Sv ($1 \text{ Sv} = 10^6 \text{ m}^3 \text{ s}^{-1}$) is perhaps slightly high relative to observations (Figure 2d). In the SO around Antarctica, the maximum overturning stream function is roughly 5 Sv. The “Antarctic Bottom Water” (AABW) that forms here covers the bottom of all the basins, with younger water underlying the older deep water in the Pacific (not shown here). In the NP, wintertime convection in the northeast corner produces shallow intermediate water that produces an overturning stream function with a maximum of about 5 Sv. Information about the deep circulation can also be deduced from the ventilation age, an idealized tracer that is set to zero at the surface, increases below the surface at the model rate (i.e., one year per model year), and is mixed and advected in the same way as temperature and salinity. From the distribution of the age tracer, one can infer the vigor of ocean ventilation at various depths and often trace the source water. In the control run, a core of young water (< 200 years old) follows the western boundary of the Atlantic at a depth of roughly 2.5 km (Figure 3). At the abyssal depths, the youngest water is located in the south, indicating its source around Antarctica. The oldest water resides around 2.5 km in the northeast Pacific while NP intermediate water forms in the eastern NP to a depth of about 1 km.

3.2. Oceanic Response to Dynamic Temperature Change

[20] The maximum values of the overturning stream function in the SO and the NP show a monotonic increase with dynamic warming (Figure 4a). This is expected because, at warmer temperatures, the density is more sensitive to temperature so that wintertime convection is stronger. In contrast, the overturning in the NA is reduced in a dynamically warm world. An overturning stream function is indicative of convection and deep water formation, but it is a zonal integral of the velocity field and is as such not identical or necessarily proportional to the rate of deep water formation. (When we speak here and in the rest of the paper of deep water formation, we include NP intermediate water formation.) The overturning varies roughly linearly with dynamic temperature change in the NA and NP. In the SO, the maximum overturning stream function is not very sensitive to dynamic temperature change at low temperatures but the sensitivity (i.e., slope) increases from $\Delta T = 4.5^{\circ}\text{C}$. This is probably because the SO is the coldest basin and, as such, is already quite insensitive to temperature gradients in the control run. A further decrease in temperature has only a small effect on the overturning.

[21] Another, perhaps more appropriate, proxy for the vigor of the large-scale deep circulation is the ventilation age. Figure 4b shows the age in each deep water formation region as a function of dynamic temperature. The age of the water in these regions are averaged across the width of each basin and poleward of 50°S or 50°N . In all cases, the top boundary is 800 m, but we chose the bottom boundary to be 5 km in the SO, 3.8 km in the NA and 2.3 km in the NP in an attempt to exclude in the average changes in the ventilation age of underlying water masses that do not

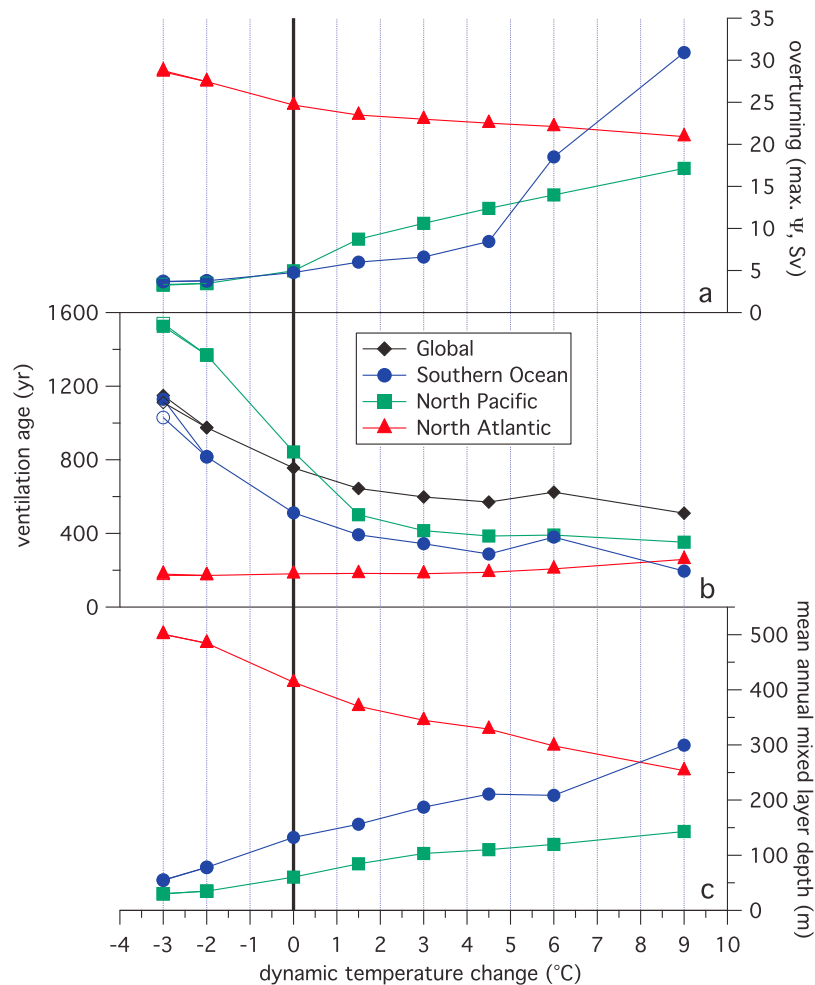


Figure 4. Sensitivity of the deep ocean circulation to dynamic temperature change in our nine experiments as indicated by the (a) overturning stream function, (b) ventilation age, and (c) mixed layer depth. All three variables are averaged across the three polar basins, poleward of 50°S or 50°N as applicable. The ventilation age was averaged vertically from 800 m down to 2.3 km in the NP, 3.8 km in the NA, and 5 km in the SO. The global ventilation age is the mean age below 800 m in the entire ocean. The experiment in which the temperature was reduced by -3°C everywhere but limited to the freezing temperature (-2°C) is indicated by circles, squares, and triangles. Because of its close correspondence with the standard $T-3^{\circ}\text{C}$ run, it is only clearly visible for the Southern Ocean ventilation age.

communicate with the surface above. The response of the ventilation tracer agrees with the stream function behavior: The SO and NP become more ventilated as the dynamic temperature goes up. Again, the change in NA overturning contrasts with the other basins. The sensitivity of the age tracer to dynamic temperature change is nonlinear, despite the almost linear response of overturning to dynamic temperature change in the NA and NP. A plausible explanation is that, in a well-mixed box, the age of water is given by $A = V/O$, where V is the volume of the box and O the (overturning) volume flux through the box. If O is linearly proportional to dynamic temperature change δT , then $A \sim 1/\delta T$, the temperature dependence of A that is shown in Figure 4b.

[22] A third and final indication of the strength of convection in the polar basins is the annual average mixed

layer depth, defined here as the depth to which the buoyancy difference with respect to the surface is less than $3 \times 10^{-4} \text{ m s}^{-2}$, and is calculated for each basin poleward of 50°S or 50°N (Figure 4c). Dynamic warming causes a deepening of the mixed layer depth in the SO and NP and a shoaling in the NA.

[23] A consistent pattern arises from the above three parameters, indicating that an increase in the thermal forcing due to a high dynamic temperature has the expected effect of creating more deep water in the SO and NP but that, surprisingly, the NA show the opposite behavior. We will discuss this response at length in section 4.1. The overall response, though, is increased global ventilation upon warming. Note that the additional experiment, in which we have limited the dynamic temperature to the freezing point (indicated by open symbols in Figure 4), is

Table 1. Ocean Atmosphere and Ice Properties for the Nine Experiments^a

ΔT , °C	Deep T, °C	Deep S, psu	ACC, $10^6 \text{ m}^3 \text{ s}^{-1}$	Precipitation, 10^{-8} m s^{-1}	Atm T, °C	Ice, 10^{12} m^2
−3 (min of −2)	4.3	34.64	149	3.40	14.4	10.8
−3	4.4	34.64	147	3.40	14.4	10.9
−2	3.8	34.63	158	3.41	14.4	10.7
0	2.4	34.59	176	3.40	14.4	11
1.5	1.7	34.56	181	3.41	14.5	10.1
3	1.5	34.54	189	3.41	14.5	9.3
4.5	1.2	34.52	198	3.41	14.6	8.3
6	0.8	34.52	215	3.41	14.6	7.7
9	−0.2	34.47	250	3.42	14.7	4.5

^a“Deep T” and “Deep S” are the true temperature and salinity, respectively, of the deep ocean averaged globally from 2700 to 5000 m. “ACC” is the transport in the Antarctic Circumpolar Current, “Precipitation” is the average annual precipitation, “Atm T” is the atmospheric surface temperature, and “Ice” is the total (annually averaged) ice extent.

barely discernable from the run in which no lower temperature limit is set (indicated by solid symbols). The similarity between the two runs at $\Delta T = -3^\circ\text{C}$ is not surprising when one considers that the density in the model equation of state is almost completely insensitive to temperature change below the freezing point (Figure 1) so that gradients in temperature below -2°C have virtually no effect on density.

[24] We next examine the sensitivity of the (real) temperature and salinity to dynamic temperature change. The purpose is twofold. First, we wish to identify the inherent feedbacks in the system. This set of experiments provides a new way of identifying feedbacks due to changes in ocean circulation in that it is the first study (that we are aware of) that varies the ocean circulation without directly changing the forcing field (through winds or boundary conditions) or the tracer fields (through mixing parameters). Second, knowledge about the tracer fields may be useful for comparison with paleoclimate data and predictions of future change.

[25] The deep ocean temperature and salinity are sensitive to the relative strength of SO versus NA deep water formation. In a dynamically warm world, the bottom is filled with cold SO water, so that the average deep ocean temperature is as low as -0.2°C in the (T+9°C) case (Table 1). The temperature of the SO deep water end-member decreases as well in order to destabilize a generally fresher surface (as discussed below). On the other hand, the dynamically cold world leads to increased ventilation of the deep ocean by NADW, resulting in very warm deep water of 4.3°C in the (T−3°C) case (Figure 5a). Similarly, the deep ocean exhibits the salty signature of NADW in the cold case but is filled with fresh water in the dynamically warm world of SO deep convection dominance (Figure 5b). An additional effect on the deep ocean salinity is through sea ice coverage. The dynamically cold world has a much higher seasonal sea ice fluctuation and the associated brine rejection and surface freshening leads to a greater net export of salt to the deep (Table 1). Also relevant to the deep ocean properties is the total amount of convection, which tends to mix fresher and colder surface water with saltier and warmer water below.

[26] As convection in fresh polar regions increases because of dynamic warming, freshwater is transported into the deep ocean, rendering the surface more salty on average.

The biggest change in surface properties occurs in the eastern NP, where increased deep water formation (upon dynamic warming) is replenished by advection of warmer salty low-latitude surface water (Figures 6a and 6b). The equivalent feedback of high-latitude warming and salinification due to meridional transport is well known in the NA (A. M. de Boer et al., Atlantic dominance of the meridional overturning circulation, submitted to *Journal of Physical Oceanography*, 2006, available at <http://lgmweb.env.uea.ac.uk/e099/>). The evaporation associated with the advection of heat adds to the salty signature in the convection region. Apart from the aforementioned changes in the eastern NP temperature, the main changes in sea surface temperature (SST) occur in the ACC region. The ACC transport, calculated as the transport through “Drake Passage,” increases from 150 Sv to 250 Sv across the span of the 12°C dynamic temperature change (Table 1), bringing more cold water north and warm water south as its meanders (i.e., its path deviates from a straight zonal flow). As a result, water in the northward flowing section of the ACC cools down in a dynamically warm world in which the ACC is stronger, while the water in the southward flowing section warms up (Figure 6a).

[27] As the ocean warms, surface current speeds are found to increase in most of the ocean with the largest changes in the western boundary regions (Figure 7). This may partly be an aspect of the enhanced meridional overturning circulation, with surface transport terms balancing subsurface transport. To the extent that a constant level of no motion applies in a given region, the increased surface velocities could also be due to enhanced shear from the larger density gradients. To see how this may work, consider the well-known thermal wind relation,

$$\rho_o f \frac{\partial u}{\partial z} = g \frac{\partial \rho}{\partial y}, \quad (1)$$

where ρ is the density, ρ_o is a reference density, f is the Coriolis parameter, u is the zonal velocity, g is the gravitational acceleration and z and y are the vertical and meridional directions [Cushman-Roisin, 1994]. If we assume a reference level at depth at which the velocities are negligible, then an increase in shear ($\partial u / \partial z$) everywhere

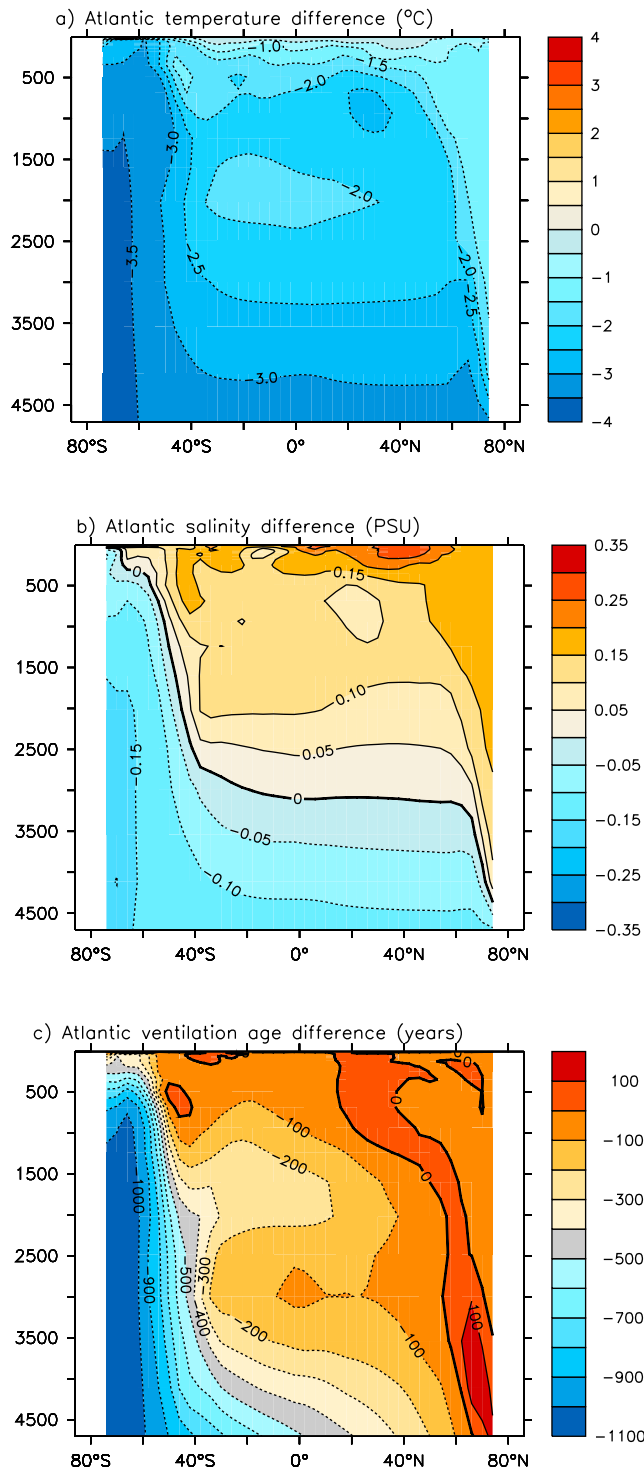


Figure 5. Zonally averaged Atlantic (a) true temperature, (b) salinity, and (c) ventilation age difference between a dynamic $T+3^{\circ}\text{C}$ state and a dynamic $T-3^{\circ}\text{C}$ state (i.e., warm-cold). As the dynamic temperature increases, ventilation is shifted from the NA to the SO, where a colder and fresher source water fills the deep ocean (Figures 5a and 5b). The increased SO deepwater formation in a dynamically warm world results in much younger water filling most of the Atlantic except in the far north where deepwater formation is reduced (Figure 5c).

above this level would result in higher surface velocities. The vertical shear will increase with dynamic temperature in the regions where the current is moving in the direction in which the temperature gradient forces it (warm water at its right in the Northern Hemisphere). The ACC and the western boundary currents in the Northern Hemisphere subtropical gyres are prominent examples. Although these currents are not in geostrophic balance in their along stream direction, they should be in the across-stream direction. A weaker ACC during the Last Glacial Maximum (LGM), as suggested by our model results, and corresponding reduction in baroclinicity may have reduced the eddy-induced transport of salty waters southward across the ACC, thus contributing to stratification in the SO. Furthermore, a

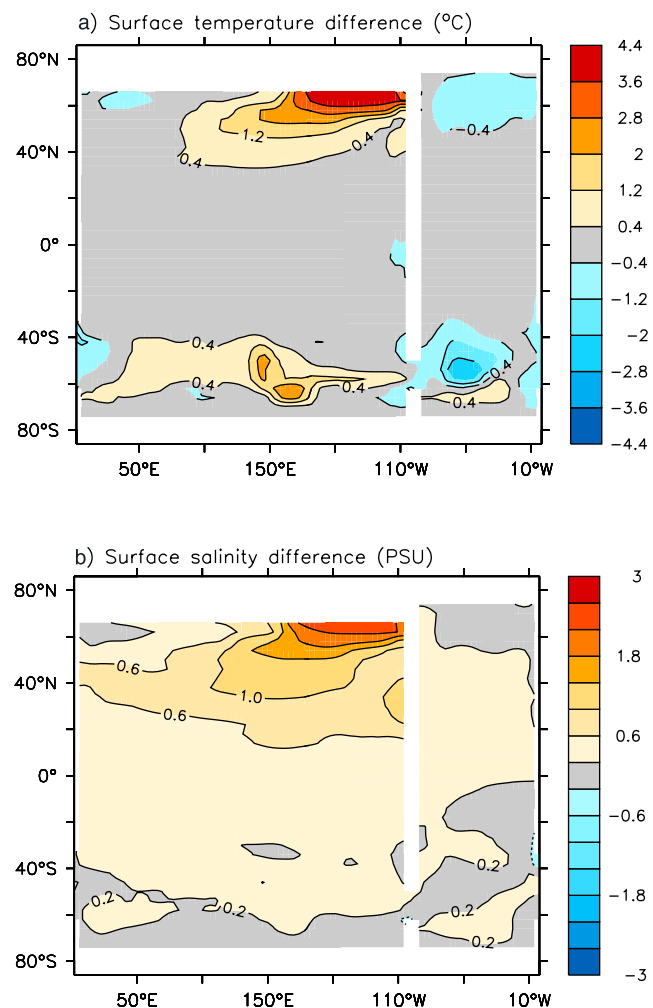


Figure 6. Difference in sea surface properties between a dynamic $T+3^{\circ}\text{C}$ state and a dynamic $T-3^{\circ}\text{C}$ state (i.e., warm-cold). The strongest response in (a) sea surface temperature and (b) sea surface salinity is in the North Pacific, where warm salty subtropical water feeds stronger intermediate water formation. The surface salinity is higher on average in a dynamic warm world, because more convection in the SO and NP transports fresh water into the deep ocean.

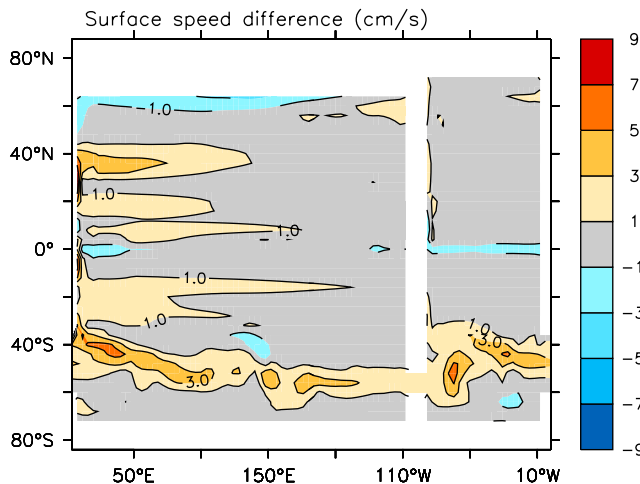


Figure 7. Surface current speed (cm s^{-1}), dynamic $T+3^{\circ}\text{C}$ minus the $T-3^{\circ}\text{C}$ case. The majority of ocean currents strengthen upon dynamic warming with the most prominent response in the ACC. Also evident is an increase in the western boundary currents.

weaker ACC would reduce the local heat transport associated with its meridional excursions. As an important caveat, the ACC transport is sensitive to the winds, and, while the winds were constant among our runs, they are not expected to remain so in a changing climate [Gnanadesikan and Hallberg, 2000].

3.3. Atmospheric and Sea Ice Response

[28] The atmospheric changes mirror the oceanic changes: As dynamic temperature is increased across the range of the experiments, the air above the convection regions warms by up to 5°C . The strongest responses are in the NP and SO, while there is no notable change in the tropics. The annual average atmospheric surface temperature increases from 14.4°C in the ($T-3^{\circ}\text{C}$) case to 14.7°C in the ($T+9^{\circ}\text{C}$) case (Table 1). Note that, although the model atmosphere only has one layer and thus one temperature per grid point, this average temperature is increased by 30°C to approximate bottom atmospheric temperatures (the calculated atmospheric temperature for the whole layer is -15.6°C). The overall rainfall does not change significantly, although a small poleward shift in the precipitation occurs with dynamic warming because the warmer atmosphere can hold and diffuse the moisture longer before it is saturated and precipitates. At the same time, the evaporation over the polar regions increases in a dynamically warm world because of the higher temperatures in the polar basins, resulting in little net change in the evaporation-precipitation difference in the polar regions. The warmer polar (SO and SNP) SST in the dynamically warmer cases has a pronounced effect on sea ice coverage, which shows a 50% decrease over the 12°C increase in dynamic temperature (Table 1). This ice retreat occurs in the NP and SO, while the NA is ice-free in all experiments. As discussed above, the brine rejection due to the larger seasonal sea ice change in the dynamically colder cases contributes to the saltier

deep ocean in those cases. In addition, the albedo effect of the sea ice has a cooling effect on the atmosphere above.

4. Discussion

4.1. Differential Responses of the Polar Ocean Regions

[29] Upon dynamic warming, convection increases markedly in regions that have strong haloclines such as the SO and the NP. Here the mean dynamic temperature increase strengthens the negative thermal buoyancy of surface water that is required to overcome the positive salinity buoyancy. As a result, the winter stratification weakens in the polar regions, allowing more deep water formation (Figure 8). The annual mean stratification increases everywhere upon dynamic warming, similar to global warming studies [Sarmiento *et al.*, 1998], but it is the winter conditions that

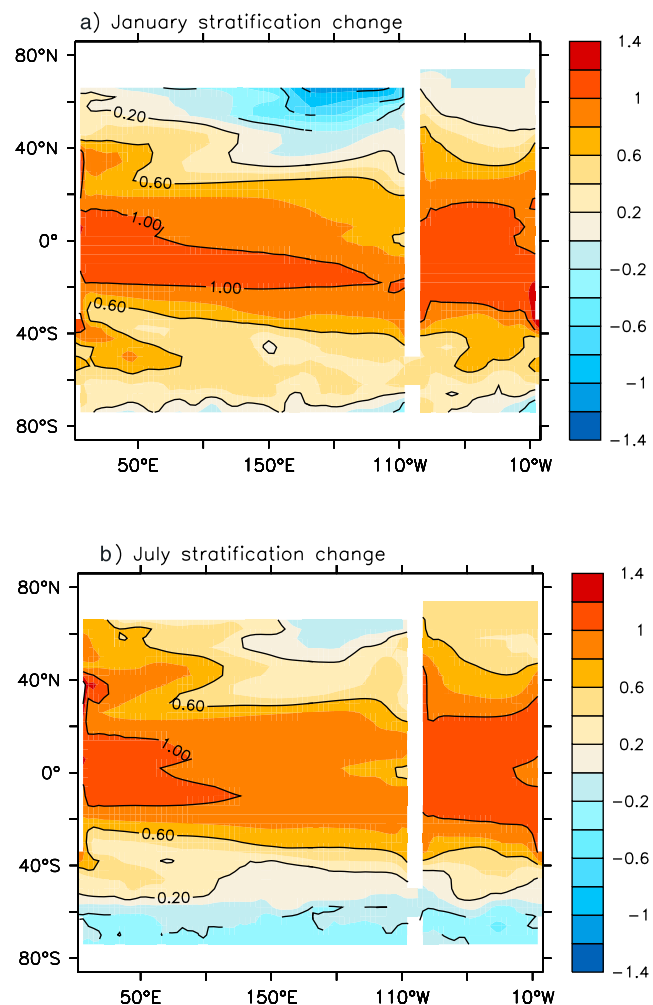


Figure 8. Surface dynamic stratification response to dynamic temperature change for (a) January and (b) July. The maps show the difference of the vertical density gradient in the upper layer (σ at 500 m minus σ at 0 m) between the dynamic $T+3^{\circ}\text{C}$ and the $T-3^{\circ}\text{C}$ cases (kg m^{-3}). In boreal winter, NP stratification decreases with dynamic warming, while SO destratification is most pronounced in the austral winter.

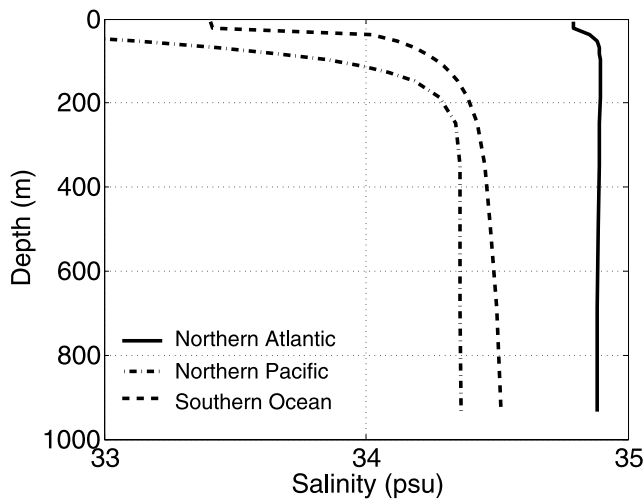


Figure 9. Depth profiles of annual average salinity in the three polar basins, averaged poleward of 50°S or 50°N for the control run. The strong halocline of the NP and SO is virtually absent in the NA.

are important for convection and thus deep ocean ventilation. Unlike the other polar basins, overturning decreases upon dynamic warming in the NA, where the positive salinity buoyancy is smallest among the polar regions. Why does convection decrease here when the thermal buoyancy forcing is more efficient? The first indication is in the vertical structure of the temperature and salinity. In regions of strong haloclines, the thermal forcing is vital: Strong cooling is required to overcome the freshwater buoyancy (Figure 9). The NA features no such strong halocline (only a weak halocline is visible in the summer), so that the water can convect there without first reaching a large negative thermal buoyancy. Dynamic temperature change affects the thermal forcing there too, but by a much smaller amount. Nevertheless, the low sensitivity of the local vertical stratification in the NA to dynamic temperature change cannot explain the marked decrease in overturning there as a result of dynamic warming ($\sim 30\%$ over the 12°C span, Figure 4a). There is no apparent reason for NADW formation to be reduced by dynamic warming because of local effects, because it does have a weak halocline, and its wintertime stratification is reduced by dynamic warming (Figure 8a). Thus we search for the answer globally.

[30] We propose that our results are the consequence of an overturning constrained by mechanical energy input [Munk and Wunsch, 1998; Wunsch and Ferrari, 2004]. For such an overturning, it is reasonable to assume that there are lower and upper constraints on the amount of deep water that forms globally, such that a strong reduction in one polar basin is compensated for by an increase in another basin. Convection and subsequent sinking of polar waters to depth necessitates that an equal amount of water rise to the surface elsewhere. The upwelling of cold deep water can occur in the SO through wind-driven divergence or at low latitudes where it is enabled by downward diffusion of heat (parameterized in our model using a constant “turbulent” vertical

diffusion coefficient). Both processes raise the ocean’s available potential energy and as such require input of energy. Winds and tides are believed to supply the energy needed, although their relative importance and the mechanisms of energy transfer are areas of active research [Nilsson *et al.*, 2003; Wunsch and Ferrari, 2004]. Nonetheless, it is reasonable to assume a nonzero lower limit and an upper limit to the upwelling through a given level. In a dynamically warm world, if an increase in the convection and sinking of NP and SO polar waters push the global convection above the upper limit sustainable by the supply of mechanical energy, convection has to decrease elsewhere, the NA in our study. Conversely, a reduction in SO and NP deep water formation that reduces the global convection below the lower limit of upwelling will force the production of more NADW.

[31] This type of anticorrelation between deep water formation regions is not new. The idea of a constraint on the deep ocean ventilation that forces AABW to form when NADW formation is shut off was proposed to explain radiocarbon observations during the last deglaciation by Broecker [1998], who described it as a “bipolar seesaw” [see also Broecker, 2000; Seidov *et al.*, 2001]. In addition to the SO-NA anticorrelation, our model exhibits an opposite tendency in the convection in the NP and NA, similar to the results of Saenko *et al.* [2004] obtained in a 1.8° latitude by and 3.6° longitude realistic topography configuration of the UVic Earth System Climate Model [Weaver *et al.*, 2001].

[32] Antiphase behavior between northern and southern polar deep water formation was also found by Winton [1997] in his study of the effect of global cooling in an idealized one-basin bihemispheric model. However, because his basin geometry and freshwater forcing rendered his northern basin the freshest one, it was this basin that stratifies upon cooling, while convection increased in his southern basin. In the modern ocean, deep water formation in the North Atlantic occurs in a much saltier region than that of AABW formation, so that we expect the response to global temperature change to be closer to what we find (i.e., stratification upon cooling in the Southern Ocean). On the other hand, during the last glacial period, the North Atlantic may have been fresher in relation to the Southern Ocean [Adkins and Schrag, 2003; Keeling and Stephens, 2001], so that the results of Winton [1997] may be relevant to the LGM (i.e., stratification upon cooling in the North Atlantic).

4.2. Constraints on Global Mean Overturning

[33] Notwithstanding the compensatory nature of the deep ventilation in the NA, NP and SO, the global deep ocean ventilation in the model appears to increase upon dynamic warming (Figure 4b). Two geographical aspects of the flow contribute to this trend. First, the mean ocean ventilation age may be more sensitive to overturning in the SO and NP than in the NA, because the first two are more proximal to the Pacific, which represents most of the volume of the ocean interior. Second, the ages of deep water in the NP and SO change more markedly than that in the NA over the parameter space of our problem so that it has a more pronounced effect on the trend of the mean age. Very old ages only occur when the overturning is almost zero (see section 3.2); even in very warm periods, this does not occur in the NA. Nevertheless,

consistent with the decreasing global ventilation age, the maxima of the stream functions in the three basins (Figure 4a) suggest that the total amount of deep water formation increases in a warm world. Why does this occur?

[34] As mentioned earlier, exactly how the total overturning depends on the mechanical energy supply is not a simple problem and is unlikely to be conclusively solved in the near future. However, we point out here that our increased overturning in a warmer world, as indicated in Figure 4, is consistent with the conventional, though somewhat outdated, scenario of an overturning circulation driven by downward mixing of buoyancy at low latitudes [Broecker, 1991; Munk, 1966]. This picture is sometimes further simplified in analytical or numerical studies by assuming that the vertical diffusivity in the ocean is horizontally and/or vertically constant and is unresponsive to the differences in ocean density structure among circulation states. Scaling analysis based on these principles indicate a $1/3$ power sensitivity of the overturning on the meridional density gradient [Welerand, 1986; Bryan, 1987] (see Appendix B). In the model, homogenous dynamic warming causes an increase in the meridional density gradient. Thus the scaling analysis would predict a stronger overturning with increased mean ocean temperature (all else being equal). A descriptive way to argue for a stronger mixing-driven overturning in a warmer world is the following. The deep ocean cannot be much lighter than the winter polar surface density (i.e., must have similar density to it) or else the polar ocean will become unstable and overturn. Thus, if there is an increase in the surface water density difference between the poles and the lower latitudes (as occurs with dynamic warming), the density difference between the equator and deep should also increase. To the extent that the increased vertical density gradient would increase downward buoyancy flux to the deep, one may expect the polar ocean overturning to increase to maintain the buoyancy balance (see auxiliary material¹). This argument can be related to the scaling argument above: Assuming a constant vertical diffusivity (as in the scaling argument), the downward buoyancy flux will increase with the high-to-low latitude surface density difference, so as to cause more overturning in a homogeneously warmer ocean.

[35] However, several caveats warn against putting great significance in the model response in global ocean ventilation or the above mixing-driven interpretation of it. First, unlike in the scaling analysis, the vertical diffusivity in our model varies with depth, in accordance with observational evidence of enhanced mixing in the deep ocean around complex bathymetry [Ledwell et al., 2000; Naveira Garabato et al., 2004]. Second, the vertical diffusivity, of order $10^{-4} \text{ m}^2 \text{ s}^{-1}$, that is needed to drive an overturning fueled by low latitude diffusive downward transport of buoyancy, is an order of magnitude larger than that typically observed in the upper ocean [Law et al., 2003; Ledwell et al., 1993]. Third, it is likely that the diffusivity is itself sensitive to the density structure and can thus adjust itself in time [Nilsson et al., 2003]. Fourth, the coarse vertical

resolution of our model introduces additional spurious numerical mixing. Last but not least, the scaling analysis assumes an enclosed basin. It is now believed that the wind-driven upwelling associated with the open channel in the Southern Ocean is a crucial component in the overturning circulation [Kuhlbrodt et al., 2007; Toggweiler and Samuels, 1995].

[36] The underlying motivation of our study is to understand the potential for abyssal ventilation changes to alter atmospheric CO_2 . In this regard, the critical issue is the importance of nutrient-rich regions such as the Antarctic and subarctic North Pacific in ventilating the interior, relative to the nutrient-poor North Atlantic [Ito and Follows, 2005; Sigman and Haug, 2003; Toggweiler et al., 2003], not the global deep ventilation rate. Thus we end this section with the reminder that, while we have much to learn about the global rate of deep ventilation, this is important in the present study only to the degree that the model response can be compared with paleoclimate data. In this regard, the results are encouraging, in that there is growing radiocarbon evidence for a globally older deep ocean during the cold conditions of the last ice age [Adkins and Boyle, 1997; Goldstein et al., 2001; Keigwin, 2004; Shackleton et al., 1988; Sikes et al., 2000].

4.3. Implications for the Glacial North Atlantic

[37] Above, we refer to observations that argue for reduced ventilation and polar stratification during cold climates. However, no community-wide consensus yet exists in favor of this interpretation [Anderson et al., 2002; Elderfield and Rickaby, 2000; Schmittner, 2003; Stephens and Keeling, 2000]. Our model results provide a physical mechanism for a link between stratification and cooling, and thus strengthen its plausibility. However, there are disagreements between our model outcome and some observations, which we address here.

[38] The most prominent data/model mismatch concerns our finding of increased NADW formation upon cooling. The available benthic foraminiferal data have been interpreted to indicate a shoaling and net reduction in overturning but not a complete shutdown [Boyle, 1997; Curry and Oppo, 1997; Keigwin, 2004], as have efforts to reconstruct geostrophic flow in the upper water column of the NA [Lynch-Stieglitz, 2001; Lynch-Stieglitz et al., 1999]. Sediment $^{231}\text{Pa}/^{230}\text{Th}$ measurements suggest that NA overturning during the last ice age was no lower than 70% of the modern flow [Marchal et al., 2000]. Our model results suggest that the NA overturning is slightly stronger during colder times, but we should also point out weaknesses in our model that could be partially responsible.

[39] First, owing to the idealized topography, the model may overestimate the strength of the anticorrelation between NA overturning and the overturning in the SO and NP. The seesaw effect depends largely on the degree of distinction in salinity conditions among these polar regions: Because the NA is less salinity-stratified (and less temperature-stratified) than the SO and NP, it is the basin that maintains the needed global ocean overturning as surface conditions become more conducive to stratification in each of the polar regions. If NA conditions were less different from the other polar surface regions, then the seesaw effect

¹Auxiliary materials are available in the HTML. doi:10.1029/2005PA001242.

would be weaker. There are some indications that the model's NA is indeed somewhat too saline (e.g., the high rate of NA overturning in the control run). In the modern case and in our model, this could be due to the neglect of a Bering Strait that acts to mix the surface properties of the NA and SNP [de Boer and Nof, 2004a, 2004b]. During the last ice age a similar freshening in the North Atlantic may have resulted from the break off of land ice or from a more southward sea ice extent.

[40] Second, our model, by design, does not include any feedbacks such as changes in the wind field. An equatorward shift in the westerly winds over the SO during cold climates [Stuut and Lamy, 2004] could explain the observed reduction in NADW formation that we are missing [Toggweiler et al., 2006]. As the westerly winds shift northward out of the Drake Passage latitude, the wind driven upwelling is reduced, countering the necessity for increased NADW formation upon SO stratification.

[41] Two other model/data conflicts regarding our deep ocean properties deserve mentioning. First, our deep ocean warms in a dynamically cold world, a response that is not observed in LGM observations. This is easily explained by the fact that we only change the temperature in the density equation and not the real temperature. In effect, we introduce the apparent temperature misfit ourselves because we do not want the feedbacks involved with real ocean temperature change. Second and more important, our results do not show a shoaling of the contact between NA- and SO-ventilated deep water in a dynamically cold world, a central observation from LGM measurements [Curry and Oppo, 2005]. This is a concern regarding the EOS hypothesis and is at least conceptually related to the model's increased NA ventilation that occurs in the dynamically cold experiments. Some previous efforts to understand the shoaling of North Atlantic ventilation during the last ice age have pointed to the regionally specific loss of "Lower North Atlantic Deep Water" formation in the Greenland-Iceland-Norwegian seas [Lehman and Keigwin, 1992; Khodri et al., 2001], possibly with continued formation of "Upper NADW" in the Labrador Sea. If such regionality is important to North Atlantic ventilation shoaling, then our model should indeed fail to capture it. On the other hand, the glacial shoaling of North Atlantic overturning in coupled climate model simulations have been interpreted as the result of an increased density contrast between North Atlantic- and Antarctic-formed deep water during the last ice age [Ganopolski et al., 1998]. If this is correct, then the failure of the dynamically cold simulations to capture the shoaling is a greater concern for the EOS hypothesis. Interestingly, in the dynamically cold simulations, salinity increases in the abyssal Atlantic, because of at least partially increased salinity in Southern Ocean-sourced deep water (Figure 5b). While the changes does not quantitatively match the observations of an extreme increase in deep Southern Ocean salinity [Adkins et al., 2002], they are in the right direction and presumably result from the need, in a dynamically colder world, for Antarctic water to be saltier before it can sink into the interior. In any case, the available data suggest that this abyssal Atlantic water was ventilated very slowly during the

LGM [Adkins et al., 2005; Keigwin, 2004], an observed change which the dynamically cold experiments do capture.

5. Conclusions

[42] Our experiments are idealized and intended to test the importance of the nonlinearity of the EOS. They clearly do not attempt to simulate the glacial climate or predict the future one. Neglected feedbacks involve, for example, wind shifts, sea ice variations, CO₂/global temperature feedbacks, the effect of land ice on the albedo, and changes to the hydrological cycle. Each of these is expected to play an important role. Thus whether our results would hold firm for a real ocean temperature change and all its corresponding feedbacks is not known. Some of the above mentioned feedbacks, such as the hydrological cycle, are likely to work against our proposed mechanism for stratifying cold polar oceans. Others, such as the carbon cycle feedbacks, will tend to reinforce it. Currently, it cannot be discerned which of these feedbacks features most prominently during global cooling or warming. Future work should focus on isolating and studying each of these feedbacks so that we can understand them mechanistically. Then their interaction and relative importance can be studied by combining them. This should ideally be done in a model that includes an explicit carbon cycle.

[43] Nevertheless, our results do indicate that reasonable changes in global oceanic temperature can have a first-order effect on the global circulation. In addition, unlike most of the feedbacks listed above, our temperature mechanism is the only one that is inextricably linked to climate; that is, unlike sea ice variations, wind shifts and precipitation changes, we know for certain the thermodynamic implications of warming and cooling (i.e., in the EOS). As such, we believe we have identified a fair candidate to explain the observed correlations among climate, polar ocean stratification, and deep ocean ventilation.

Appendix A: Description of the Energy Moisture Balance Model

[44] The EMBM used for this study solves prognostically for the atmospheric temperature and specific humidity. Apart from initialization and diagnostic routines, it is composed mainly of three physical parts, namely the radiation, precipitation and diffusion subroutines.

[45] In the radiation routine, the longwave and shortwave radiation fluxes are computed. The daily mean latitudinally varying solar radiation is derived using a solar constant of 1360 W m⁻². This radiation is then reduced at the top and bottom of the atmosphere according to (user specified) coefficients for atmospheric reflectivity and absorption and the albedo. The longwave radiation is calculated from Stephan-Boltzmann's law. In the computation of the outgoing longwave radiation at the top of the atmosphere, the mean atmospheric temperature is used. For calculating the downward longwave radiation at the bottom of the atmospheric layer, the atmospheric temperature is increased by 20°C (to artificially introduce a temperature gradient across the layer). Upward longwave radiation into the atmospheric

layer is calculated using the input surface temperatures from the ice and land models. The net sum of the radiative fluxes is divided by the heat capacity of the air and the mass of the layer to give the rate of temperature increase.

[46] The second routine computes the precipitation. First, the saturation mixing ratio is calculated at an estimated bottom atmospheric temperature, set to be the mean atmospheric temperature plus a user specified value (typically 30°C). If the model mixing ratio exceed the saturation mixing ratio and the lower atmospheric temperature is above freezing, liquid precipitation forms in the following way:

$$lp = -((qs - q)/(1 + lcp * dqt)) * (m/dt),$$

where lp is the liquid precipitation, q_s is the saturation mixing ratio, q is the model mixing ratio in the lower atmosphere, lcp is the latent heat of evaporation divided by the heat capacity of air, dqt is the derivative of the saturation mixing ratio to temperature, m is the mass of the layer and dt is the time step. Frozen precipitation is similarly derived when the lower atmospheric temperature is below freezing point except that the latent heat of fusion is added to the latent heat of evaporation. The transformation of water vapor to liquid precipitation also changes the atmospheric temperature, T_a , by an amount,

$$T_a = -lcp * (qs - q)/(1 + lcp * dqt).$$

The calculation of the temperature change due to frozen precipitation again includes the latent heat of fusion.

[47] In the third major routine, temperature and humidity is laterally diffused (in all directions). A uniform diffusion coefficient of $10 \text{ m}^2 \text{ s}^{-1}$ is applied. The EMBM is called by the main coupler code in the same way as a full-scale atmospheric model. Thus the model computes the radiation balance during a downward sweep of a standard tridiagonal solver and then computes the precipitation and diffusion during the upward sweep.

Appendix B: Scaling Analyses

[48] For completeness, we briefly repeat the scaling analysis of *Wendler* [1986] and others that lead to an increased meridional overturning because of increased

meridional density gradients. Consider a scaling of the thermal wind equation (1),

$$L_y \rho_0 f U = \Delta \rho g H, \quad (\text{B1})$$

where U is the zonal velocity scale, f is a typical value (say midlatitude) for the Coriolis parameter, L_y is the meridional length scale, H is a typical vertical scale such as the thermocline depth, ρ_0 is a reference density and $\Delta \rho$ is the meridional density difference. Mass conservation and the assumption that $U \sim V$, the meridional scale velocity, implies that,

$$VH = WL_y, \quad (\text{B2})$$

where W is a typical vertical velocity. Equating U and V and eliminating them from these two scaling equations yields

$$H^2 = L^2 \rho_0 f W / (g \Delta \rho). \quad (\text{B3})$$

If one further assumes that the ocean interior is in an vertical advective-diffusive balance and that the diffusivity coefficient is independent of depth, then scaling analysis give the relation,

$$W = K_v / H, \quad (\text{B4})$$

where K_v is the vertical diffusivity. An expression for W in terms of $\Delta \rho$ can now be obtained by eliminating H from (B3) and (B4),

$$W^3 = (g K_v^2 \Delta \rho) / (\rho_0 f L^2).$$

The increased upwelling due to the meridional density gradient is usually thought off as an indicator of increased meridional overturning.

[49] **Acknowledgments.** This study was partly supported by the U.S. National Science Foundation through awards OCE-0081686 and OCE-0136449 to D.M.S. A.M. de B. also gratefully acknowledges funding from the U.S. NOAA Geophysical Fluid Dynamics Laboratory and Princeton University's Atmospheric and Oceanic Sciences Postdoctoral Fellowship Program and the Princeton Cooperative Institute for Climate Science. Jess Adkins and an anonymous reviewer provided input that significantly improved the content of the manuscript.

References

- Adkins, J. F., and E. A. Boyle (1997), Changing atmospheric $\Delta^{14}\text{C}$ and the record of deep water paleoventilation ages, *Paleoceanography*, *12*, 337–344.
- Adkins, J. F., and D. P. Schrag (2003), Reconstructing Last Glacial Maximum bottom water salinities from deep-sea sediment pore fluid profiles, *Earth Planet. Sci. Lett.*, *216*, 109–123.
- Adkins, J. F., et al. (2002), The salinity, temperature, and delta O-18 of the glacial deep ocean, *Science*, *298*, 1769–1773.
- Adkins, J. F., et al. (2005), Rapid climate change and conditional instability of the glacial deep ocean from the thermobaric effect and geothermal heating, *Quat. Sci. Rev.*, *24*, 581–594.
- Anderson, R. F., et al. (2002), The Southern Ocean's biological pump during the Last Glacial Maximum, *Deep Sea Res., Part II*, *49*, 1909–1938.
- Bjornsson, H., and J. R. Toggweiler (2001), The climatic influence of Drake Passage, in *Oceans and Rapid Climate Change: Past, Present, and Future*, *Geophys. Monogr. Ser.*, vol. 126, edited by D. Seidov, B. J. Haupt, and M. Maslin, pp. 243–259, AGU, Washington, D. C.
- Boyle, E. A. (1997), Characteristics of the deep ocean carbon system during the past 150000 years: Sigma CO_2 distributions, deep water flow patterns, and abrupt climate change, *Proc. Natl. Acad. Sci. U. S. A.*, *94*, 8300–8307.
- Boyle, E. A., and L. D. Keigwin (1982), Deep circulation of the North-Atlantic over the last 200,000 years: Geochemical evidence, *Science*, *218*, 784–787.

- Broecker, W. S. (1991), The great ocean conveyor, *Oceanography*, 4, 79–89.
- Broecker, W. S. (1998), Paleoocean circulation during the last deglaciation: A bipolar seesaw?, *Paleoceanography*, 13, 119–121.
- Broecker, W. S. (2000), Was a change in thermohaline circulation responsible for the Little Ice Age?, *Proc. Natl. Acad. Sci. U. S. A.*, 97, 1339–1342.
- Broecker, W. S., et al. (2004), Glacial ventilation rates for the deep Pacific Ocean, *Paleoceanography*, 19, PA2002, doi:10.1029/2003PA000974.
- Brunelle, B. G., et al. (2007), Evidence from diatom-bound nitrogen isotopes for subarctic Pacific stratification during the last ice age and a link to North Pacific denitrification changes, *Paleoceanography*, 22, PA1215, doi:10.1029/2005PA001205.
- Bryan, F. (1987), Parameter sensitivity of primitive equation ocean general circulation models, *J. Phys. Oceanogr.*, 17, 970–985.
- Bryan, K., and L. J. Lewis (1979), Water mass model of the world ocean, *J. Geophys. Res.*, 84, 2503–2517.
- Charles, C. D., and R. G. Fairbanks (1992), Evidence from Southern Ocean sediments for the effect of North-Atlantic deep-water flux on climate, *Nature*, 355, 416–419.
- Curry, W. B., and D. W. Oppo (1997), Synchronous, high-frequency oscillations in tropical sea surface temperatures and North Atlantic Deep Water production during the last glacial cycle, *Paleoceanography*, 12, 1–14.
- Curry, W. B., and D. W. Oppo (2005), Glacial water mass geometry and the distribution of $\delta^{13}\text{C}$ of ΣCO_2 in the western Atlantic Ocean, *Paleoceanography*, 20, PA1017, doi:10.1029/2004PA001021.
- Cushman-Roisin, B. (1994), *Introduction to Geophysical Fluid Dynamics*, Prentice-Hall, Upper Saddle River, N. J.
- de Boer, A. M., and D. Nof (2004a), The Bering Strait's grip on the Northern Hemisphere climate, *Deep Sea Res., Part I*, 51, 1347–1366.
- de Boer, A. M., and D. Nof (2004b), The exhaust valve of the North Atlantic, *J. Clim.*, 17, 417–422.
- Elderfield, H., and R. E. M. Rickaby (2000), Oceanic Cd/P ratio and nutrient utilization in the glacial Southern Ocean, *Nature*, 405, 305–310.
- Francois, R., et al. (1997), Contribution of Southern Ocean surface-water stratification to low atmospheric CO_2 concentrations during the last glacial period, *Nature*, 389, 929–935.
- Ganopolski, A., et al. (1998), Simulation of modern and glacial climates with a coupled global model of intermediate complexity, *Nature*, 391, 351–356.
- Gent, P. R., and J. C. McWilliams (1990), Isopycnal mixing in ocean circulation models, *J. Phys. Oceanogr.*, 20, 150–155.
- Gerdes, R., et al. (2006), Sensitivity of a global ocean model to increased run-off from Greenland, *Ocean Modell.*, 12, 416–435.
- Gildor, H., et al. (2002), Sea ice switch mechanism and glacial-interglacial CO_2 variations, *Global Biogeochem. Cycles*, 16(3), 1032, doi:10.1029/2001GB001446.
- Gnanadesikan, A., and R. W. Hallberg (2000), On the relationship of the Circumpolar Current to Southern Hemisphere winds in coarse-resolution ocean models, *J. Phys. Oceanogr.*, 30, 2013–2034.
- Goldstein, S. J., et al. (2001), Uranium-series and radiocarbon geochronology of deep-sea corals: Implications for Southern Ocean ventilation rates and the oceanic carbon cycle, *Earth Planet. Sci. Lett.*, 193, 167–182.
- Griffies, S. M. (1998), The Gent-McWilliams skew flux, *J. Phys. Oceanogr.*, 28, 831–841.
- Griffies, S. M., et al. (2003), A technical guide to MOM4, technical report, NOAA Geophys. Fluid Dyn. Lab. Ocean Group, Princeton, N. J. (Available at <http://www.gfdl.noaa.gov/~fms/>)
- Haug, G. H., et al. (1999), Onset of permanent stratification in the subarctic Pacific Ocean, *Nature*, 401, 779–782.
- Haug, G. H., et al. (2005), North Pacific seasonality and the glaciation of North America 2.7 million years ago, *Nature*, 433, 821–825.
- Hodell, D. A., and K. A. Venz-Curtis (2006), Late Neogene history of deepwater ventilation in the Southern Ocean, *Geochem. Geophys. Geosyst.*, 7, Q09001, doi:10.1029/2005GC001211.
- Hughen, K., et al. (2004), ^{14}C activity and global carbon cycle changes over the past 50000 years, *Science*, 303, 202–207.
- Ito, T., and M. J. Follows (2005), Preformed phosphate, soft tissue pump and atmospheric CO_2 , *J. Mar. Res.*, 63, 813–839.
- Jaccard, S. L., et al. (2005), Glacial/interglacial changes in subarctic North Pacific stratification, *Science*, 308, 1003–1006.
- Keeling, R. F., and B. B. Stephens (2001), Antarctic sea ice and the control of Pleistocene climate instability, *Paleoceanography*, 16, 112–131.
- Keigwin, L. D. (2004), Radiocarbon and stable isotope constraints on Last Glacial Maximum and Younger Dryas ventilation in the western North Atlantic, *Paleoceanography*, 19, PA4012, doi:10.1029/2004PA001029.
- Khodri, M., Y. Leclainche, G. Ramstein, P. Braconnot, O. Marti, and E. Cortijo (2001), Simulating the amplification of orbital forcing by ocean feedbacks in the last glaciation, *Nature*, 410, 570–574.
- Knox, F., and M. B. McElroy (1984), Changes in atmospheric CO_2 : Influence of the marine biota at high latitude, *J. Geophys. Res.*, 89, 4629–4637.
- Kuhlbrodt, T., et al. (2007), On the driving processes of the oceanic meridional overturning circulation, *Rev. Geophys.*, 45, RG2001, doi:10.1029/2004RG000166.
- Law, C. S., E. R. Abraham, A. J. Watson, and M. I. Liddicoat (2003), Vertical eddy diffusion and nutrient supply to the surface mixed layer of the Antarctic Circumpolar Current, *J. Geophys. Res.*, 108(C8), 3272, doi:10.1029/2002JC001604.
- Ledwell, J. R., et al. (1993), Evidence for slow mixing across the pycnocline from an open-ocean tracer-release experiment, *Nature*, 364, 701–703.
- Ledwell, J. R., et al. (2000), Evidence for enhanced mixing over rough topography in the abyssal ocean, *Nature*, 403, 179–182.
- Lehman, S. J., and L. D. Keigwin (1992), Sudden changes in North Atlantic circulation during the last deglaciation, *Nature*, 356, 757–762.
- Lynch-Stieglitz, J. (2001), Using ocean margin density to constrain ocean circulation and surface wind strength in the past, *Geochem. Geophys. Geosyst.*, 2(12), doi:10.1029/2001GC000208.
- Lynch-Stieglitz, J., et al. (1999), Weaker Gulf Stream in the Florida straits during the last glacial maximum, *Nature*, 402, 644–648.
- Manabe, S., and R. J. Stouffer (1993), Two stable equilibria of a coupled ocean atmosphere model—Reply, *J. Clim.*, 6, 178–179.
- Manabe, S., and R. J. Stouffer (1997), Coupled ocean-atmosphere model response to freshwater input: Comparison to Younger Dryas event, *Paleoceanography*, 12, 728.
- Marchal, O., R. François, T. F. Stocker, and F. Joos (2000), Ocean thermohaline circulation and sedimentary $^{231}\text{Pa}/^{230}\text{Th}$ ratio, *Paleoceanography*, 15, 625–641.
- McDougall, T. J., et al. (2003), Accurate and computationally efficient algorithms for potential temperature and density of seawater, *J. Atmos. Oceanic Technol.*, 20, 730–741.
- Milly, P. C. D., and A. B. Shmakin (2002), Global modeling of land water and energy balances. part I: The land dynamics (LaD) model, *J. Hydrometeorol.*, 3, 283–299.
- Munk, W. (1966), Abyssal recipes, *Deep Sea Res., Part I*, 13, 207–230.
- Munk, W., and C. Wunsch (1998), Abyssal recipes II: Energetics of tidal and wind mixing, *Deep Sea Res., Part I*, 45, 1977–2010.
- Naveira Garabato, A. C., et al. (2004), Widespread intense turbulent mixing in the Southern Ocean, *Science*, 303, 210–213.
- Nilsson, J., et al. (2003), The thermohaline circulation and vertical mixing: Does weaker density stratification give stronger overturning?, *J. Phys. Oceanogr.*, 33, 2781–2795.
- Ninnemann, U. S., and C. D. Charles (2002), Changes in the mode of Southern Ocean circulation over the last glacial cycle revealed by foraminiferal stable isotopic variability, *Earth Planet. Sci. Lett.*, 201, 383–396.
- Rahmstorf, S., and A. Ganopolski (1999), Long-term global warming scenarios computed with an efficient coupled climate model, *Clim. Change*, 43, 353–367.
- Ravelo, A. C., and D. H. Andreasen (2000), Enhanced circulation during a warm period, *Geophys. Res. Lett.*, 27, 1001–1004.
- Redi, M. H. (1982), Oceanic isopycnal mixing by coordinate rotation, *J. Phys. Oceanogr.*, 12, 1154–1158.
- Robinson, R. S., et al. (2004), Revisiting nutrient utilization in the glacial Antarctic: Evidence from a new method for diatom-bound N isotopic analysis, *Paleoceanography*, 19, PA3001, doi:10.1029/2003PA000996.
- Roske, F. (2006), A global heat and freshwater forcing dataset for ocean models, *Ocean Modell.*, 11, 235–297.
- Saenko, O. A., et al. (2004), The Atlantic-Pacific seesaw, *J. Clim.*, 17, 2033–2038.
- Sarmiento, J. L., and J. R. Toggweiler (1984), A New model for the role of the oceans in determining atmospheric $p\text{CO}_2$, *Nature*, 308, 621–624.
- Sarmiento, J. L., et al. (1998), Simulated response of the ocean carbon cycle to anthropogenic climate warming, *Nature*, 393, 245–249.
- Schmittner, A. (2003), Southern Ocean sea ice and radiocarbon ages of glacial bottom waters, *Earth Planet. Sci. Lett.*, 213, 53–62.
- Seidov, D., et al. (2001), Ocean bi-polar seesaw and climate: Southern versus northern meltwater impacts, in *Oceans and Rapid Climate Change: Past, Present, and Future*, *Geophys. Monogr. Ser.*, vol. 126, edited by D. Seidov, B. J. Haupt, and M. Maslin, pp. 169–197, AGU, Washington, D. C.
- Shackleton, N. J., et al. (1988), Radiocarbon age of last glacial Pacific deep-water, *Nature*, 335, 708–711.
- Siegenthaler, U., and T. Wenk (1984), Rapid atmospheric CO_2 variations and ocean circulation, *Nature*, 308, 624–626.
- Sigman, D. M., and G. H. Haug (2003), The biological pump in the past, in *Treatise on Geochemistry*, vol. 6, *The Oceans and Marine*

- Geochemistry*, pp. 491–528, Elsevier, New York.
- Sigman, D. M., et al. (2004), Polar ocean stratification in a cold climate, *Nature*, **428**, 59–63.
- Sikes, E. L., et al. (2000), Old radiocarbon ages in the southwest Pacific Ocean during the last glacial period and deglaciation, *Nature*, **405**, 555–559.
- Steele, M., et al. (2001), PHC: A global ocean hydrography with a high-quality Arctic Ocean, *J. Clim.*, **14**, 2079–2087.
- Stephens, B. B., and R. F. Keeling (2000), The influence of Antarctic sea ice on glacial-interglacial CO₂ variations, *Nature*, **404**, 171–174.
- Stouffer, R. J., and S. Manabe (2003), Equilibrium response of thermohaline circulation to large changes in atmospheric CO₂ concentration, *Clim. Dyn.*, **20**, 759–773.
- Stuut, J. B. W., and F. Lamy (2004), Climate variability at the southern boundaries of the Namib (southwestern Africa) and Atacama (northern Chile) coastal deserts during the last 120000 yr, *Quat. Res.*, **62**, 301–309.
- Toggweiler, J. R. (1999), Variation of atmospheric CO₂ by ventilation of the ocean's deepest water, *Paleoceanography*, **14**, 571–588.
- Toggweiler, J. R., and B. Samuels (1995), Effect of Drake Passage on the global thermohaline circulation, *Deep Sea Res., Part I*, **42**, 477–500.
- Toggweiler, J. R., A. Gnanadesikan, S. Carson, R. Mumane, and J. L. Sarmiento (2003), Representation of the carbon cycle in box models and GCMs: 1. Solubility pump, *Global Biogeochem. Cycles*, **17**(1), 1026, doi:10.1029/2001GB001401.
- Toggweiler, J. R., J. L. Russell, and S. R. Carson (2006), Midlatitude westerlies, atmospheric CO₂, and climate change during the ice ages, *Paleoceanography*, **21**, PA2005, doi:10.1029/2005PA001154.
- Trenberth, K. E., et al. (1990), The mean annual cycle in global ocean wind stress, *J. Phys. Oceanogr.*, **20**, 1742–1760.
- Wang, Z. M., L. A. Mysak, and J. F. McManus (2002), Response of the thermohaline circulation to cold climates, *Paleoceanography*, **17**(1), 1006, doi:10.1029/2000PA000587.
- Weaver, A. J., et al. (2001), The UVic Earth System Climate Model: Model description, climatology, and applications to past, present and future climates, *Atmos. Ocean*, **39**, 361–428.
- Welander, P. (1986), Thermohaline effects in the ocean circulation and related simple models, in *Large-Scale Transport Processes in Oceans and Atmosphere*, edited by J. Willebrand and D. L. T. Anderson, pp. 163–200, Springer, New York.
- Winton, M. (1997), The effect of cold climate upon North Atlantic Deep Water formation in a simple ocean-atmosphere model, *J. Clim.*, **10**, 37–51.
- Winton, M. (2000), A reformulated three-layer sea ice model, *J. Atmos. Oceanic Technol.*, **17**, 525–531.
- Wunsch, C., and R. Ferrari (2004), Vertical mixing, energy and the general circulation of the oceans, *Annu. Rev. Fluid Mech.*, **36**, 281–314.

A. M. de Boer, School of Environmental Science, University of East Anglia, Norwich, NR4 7TJ, UK. (a.deboer@uea.ac.uk)

J. L. Russell, Department of Geosciences, University of Arizona, Tucson, AZ 85721, USA.

D. M. Sigman, Department of Geosciences, Princeton University, Princeton, NJ 08544, USA.

J. R. Toggweiler, Geophysical Fluid Dynamics Laboratory, NOAA, Princeton, NJ 08542, USA.